A P_2-P_1 PARTIALLY PENALIZED IMMERSED FINITE ELEMENT METHOD FOR STOKES INTERFACE PROBLEMS

YUAN CHEN AND XU ZHANG

Abstract. In this article, we develop a Taylor-Hood immersed finite element (IFE) method to solve two-dimensional Stokes interface problems. The $\mathcal{P}_2$-$\mathcal{P}_1$ local IFE spaces are constructed using the least-squares approximation on an enlarged fictitious element. The partially penalized IFE method with ghost penalty is employed for solving Stoke interface problems. Penalty terms are imposed on both interface edges and the actual interface curves. Ghost penalty terms are enforced to enhance the stability of the numerical scheme, especially for the pressure approximation. Optimal convergences are observed in various numerical experiments with different interface shapes and coefficient configurations. The effects of the ghost penalty and the fictitious element are also examined through numerical experiments.

Key words. Stokes interface problem, immersed finite element method, fictitious element, least-squares.

1. Introduction

In this paper, we consider the steady-state Stokes interface problem in the two-dimensional case. Let $\Omega \subset \mathbb{R}^2$ be an open bounded domain that is separated into Ω^+ and Ω^- by a smooth interface curve Γ. Consider the following Stokes equation in the velocity-pressure-stress form

$$-\nabla \cdot \sigma(\mathbf{u}, p) = \mathbf{f}, \text{ on } \Omega^+ \cup \Omega^-, \tag{1a}$$

$$\nabla \cdot \mathbf{u} = 0, \text{ on } \Omega^+ \cup \Omega^-, \tag{1b}$$

$$\mathbf{u} = \mathbf{0}, \text{ on } \partial\Omega. \tag{1c}$$

Here, $\mathbf{f}$ is given body force. $\mathbf{u}$ represents flow velocity field of an incompressible fluid motion, and p denotes the pressure. $\sigma(\mathbf{u}, p)$ is the stress tensor defined by

$$\sigma(\mathbf{u}, p) = 2\nu\boldsymbol{\epsilon}(\mathbf{u}) - p\mathbf{I} \tag{1d}$$

where the strain tensor $\boldsymbol{\epsilon}(\mathbf{u}) = \frac{1}{2}(\nabla\mathbf{u} + (\nabla\mathbf{u})^t)$. Across the interface Γ, the viscosity coefficient $\nu(\mathbf{x})$ is discontinuous. Without loss of generality, we assume that ν is a piecewise constant function as follows:

$$\nu = \begin{cases} \nu^+, & \text{in } \Omega^+, \\ \nu^-, & \text{in } \Omega^-. \end{cases} \tag{1e}$$

Across the interface Γ, the following jump conditions are enforced:

$$[\![\mathbf{u}]\!]_\Gamma = \mathbf{0}, \text{ on } \Gamma, \tag{1f}$$

$$[\![\sigma(\mathbf{u}, p)\mathbf{n}]\!]_\Gamma = \mathbf{0}, \text{ on } \Gamma, \tag{1g}$$

where the jump $[\![\mathbf{w}(\mathbf{x})]\!]_\Gamma = \mathbf{w}^+(\mathbf{x})|_\Gamma - \mathbf{w}^-(\mathbf{x})|_\Gamma$, and $\mathbf{n}$ is the unit normal vector on Γ pointing from Ω^- to Ω^+.

The Stokes equation is a linearization of the well-known Navier-Stokes equation. Stokes interface problems often describe multiphase flow with jumps in velocity, pressure, and physical parameters. Simulations of multiphase flow are widely applied in fields of fluid dynamics and biology. Examples of these applications include water-oil flow, bubble column reactors, drug delivery, treatment of lung diseases, and polymer blending and polymer electrolyte membrane fuel cell [28], etc.

PDE Interface problems, including aforementioned Stokes interface problem, have attracted great attention among mathematicians, computational scientists and engineers in the past decades. A wide variety of numerical methods, particularly finite element method (FEM), have been developed and matured for solving interface problems. There are roughly two classes of FEM when it comes to interface problems, namely the fitted-mesh FEM and the unfitted-mesh FEM. The fitted-mesh method, such as the conventional FEM, requires the solution mesh to be aligned with the interface; otherwise, the convergence of the numerical method could be compromised. However, this body-fitting restriction limits its applicability from problems involving a moving interface, as the solution mesh needs to be regenerated at each time level. On the contrast, unfitted-mesh methods usually alleviate or even eliminate the restriction on mesh. Structured meshes, such as Cartesian meshes, are usually adopted to solve interface problems with nontrivial interface shape. See Figure 1 for an illustration of a comparison of an unfitted Cartesian mesh and a fitted-mesh with a circular interface. This property is particularly advantageous for moving interface problems [5, 27, 30]. Numerical methods falling to this class include generalized FEM [7], extended FEM (XFEM) [15], CutFEM [23] and immersed FEM (IFEM) [34], to name only a few.
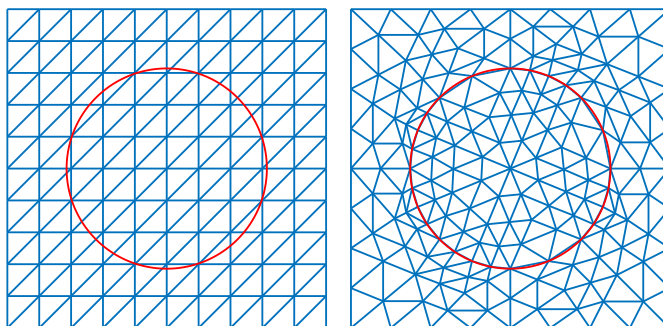

FIGURE 1. Non-body fitting (left) and body-fitting (right) meshes.

The idea of immersed finite element method [34] is to locally modify the standard FEM basis functions around the interface to satisfiy specific interface jump conditions from the physical laws. Piecewise polynomials are developed as new basis functions on all elements intersected by interfaces. Several literatures [11, 12, 26, 27, 31, 38, 44] expand this idea to multi-dimensional elliptic interface problems and higher-order approximation. Due to the discontinuity of IFE functions across the element boundaries, a partially penalized immersed finite element method (PPIFEM) was proposed in [36] as an improvement of classical IFEM. The authors added penalty terms on interface-intersected edges to the IFE scheme to enhance its stability. Many research papers on IFEM follow this idea in the recent years. For

example, the PPIFEM has been applied to the elasticity equation [19], interface problems with triple-junction points [13], higher-order approximations [6, 17], the Helmholtz equation [20, 37] and the three-dimensional interface problems [18, 22], parabolic interface problems [39] and hyperbolic interface problems [48]. An improved *a priori* error estimation with lower regularity requirement was reported in [21] and the *a posteriori* error estimation was developed in [25].

There are a few unfitted-mesh methods developed for Stokes interface problems, such as CutFEM [24], Nitsche's Extended FEM [45], Extended FEM [16], Fictitious domain FEM [40, 42], immersed interface method [35]. Within the IFE framework, [4] proposed an immersed discontinuous Galerkin method based on broken $\mathcal{Q}_1$-$\mathcal{Q}_0$ element pair and applied the method in Stokes moving interface problem [5]. Recently [29] introduced a nonconforming IFE method based on broken CR-$\mathcal{P}_0$ and rotated $\mathcal{Q}_1$-$\mathcal{Q}_0$ pairs. A mixed conforming-nonconforming $\mathcal{P}_1$ IFE method for unsteady moving-interface Stokes interface problems was introduced in [30].

So far, to the best of our knowledge, all the IFEMs for the Stokes interface problem focused on low-order approximations, i.e., $\mathcal{P}_1$ or $\mathcal{Q}_1$ approximation for velocity and $\mathcal{P}_0$ approximation for pressure. Classical Taylor-Hood $\mathcal{P}_k$-$\mathcal{P}_{k-1}$ finite element ($k > 1$) [9, 43] has not been explored in the immersed finite element framework. The major obstacle is to construct a broken high-order immersed finite element space based on actual interface curve together with interface conditions involving both velocity and pressure on actual interface. For high-order IFE approximations, most attempts focus on elliptic interface problems. Some early work explored quadratic and higher order method on linear [2] and quadratic interface [8]. In [3], the authors enforced interface conditions using the L^2 inner product defined on the actual interface curve. Theoretical work of this method has not been developed including existence of basis functions. In [17], the authors proposed a high-order IFE space for elliptic interface problem constructed by locally solving a Cauchy problem. To handle the heavily coupled interface conditions of Stokes interface problem, we adopt the idea from least-squares high-order IFEM [6, 49] which enforces interface conditions on basis functions in a least-squares sense. The existence of the IFE shape functions is guaranteed by the nature of least squares.

Another concern in Stokes interface problems is the ill-conditioning of the linear system of the saddle-point problem. To overcome this issue, we follow the idea of ghost penalty [10] which is applied in XFEM [33, 32], Nitsche's method [46], CutFEM [14, 24, 41] for solving Stokes interface problems. The technique is also a necessary ingredient in theoretically estabiliing the inf-sup conditions of the aforementioned methods. The basic idea is to add extra stabilization terms on edges cut by the interface or boundary in order to control the jump of discrete polynomials in a least-squares sense. We include ghost penalty terms of both velocity and pressure in our weak formulation. Numerical examples are provided to demonstrate the necessity of these terms.

In this paper, we propose a high-order Taylor-Hood IFE method. The method uses piecewise $\mathcal{P}_2$ approximation for the velocity and piecewise $\mathcal{P}_1$ approximation for the pressure. A least-squares technique is defined on actual interface to weakly enforce the coupled interface jump conditions and incompressibility conditions. Properties of the Taylor-Hood IFE basis functions, such as the existence of the basis functions, and the their approximation capability are analyzed. The IFE functions

are used in a partially penalized IFE scheme with ghost penalty for solving the Stokes interface problems.

The rest of this paper is organized as follows. In Section 2, we construct the vector-valued IFE spaces based on least-squares and investigate some basic properties of the new IFE spaces. In Section 3, we present the partially penalized IFE method with ghost penalty for solving Stokes interface problems. In Section 4, we provide several numerical examples to demonstrate the performance of this method. A brief conclusion is given in Section 5.

2. Immersed Taylor-Hood Finite Element Spaces

In this section, we first introduce some basic notations and assumptions, and then construct the $\mathcal{P}_2$-$\mathcal{P}_1$ IFE space based on the least-squares framework.

2.1. Notations and Preliminaries. Assume from now on that Ω is a polygonal domain, and $\mathcal{T}_h$ is a regular triangulation independent of the location of the interface. Denote by $\mathcal{N}_h$ and $\mathcal{E}_h$ the set of nodes and edges of the mesh $\mathcal{T}_h$, respectively. Let $\mathcal{T}_h^i = \{T \in \mathcal{T}_h : T \cap \Gamma \neq \emptyset\}$ be the collection of interface elements. The collection of non-interface elements are denoted by $\mathcal{T}_h^n = \mathcal{T}_h \backslash \mathcal{T}_h^i$. Similarly, we define $\mathcal{E}_h^i = \{e \in \mathcal{E}_h, e \cap \Gamma \neq \emptyset\}$ and $\mathcal{E}_h^n = \mathcal{E}_h \backslash \mathcal{E}_h^i$ to be the set of interface edges and non-interface edges, respectively. The set of interior edges and boundary edges are denoted by $\mathring{\mathcal{E}}_h$ and $\mathcal{E}_h^b$, respectively. Regarding the regularity of the interface and mesh requirement, we employ similar hypotheses as stated in [6]:

- **(H1)** The interface Γ cannot intersect an edge of any element at more than two points unless the edge is part of Γ.
- **(H2)** If Γ intersects the boundary of an element at two points, these intersection points must be on different edges of this element.
- **(H3)** The interface Γ is a piecewise C^2 function, and the mesh $\mathcal{T}_h$ is formed such that on every interface element $T \in \mathcal{T}_h^i$, $\Gamma \cap T$ is C^2.

Associated with each edge $e \in \mathcal{E}_h$, a unit normal vector $\mathbf{n}_e$ is assigned. For each internal edge $e \in \mathring{\mathcal{E}}_h$ shared by two elements, denoted by $T_{e,1}$ and $T_{e,2}$, the normal $\mathbf{n}_e$ is pointing from $T_{e,1}$ to $T_{e,2}$. For a scalar function w or a vector-valued function $\mathbf{w}$ defined on $T_{e,1} \cup T_{e,2}$, we define the jump and average to be

(2)
$$[\![w]\!]_e = w|_{T_{e,1}} - w|_{T_{e,2}}, \ \{\!\{w\}\!\}_e = \frac{1}{2}(w|_{T_{e,1}} + w|_{T_{e,2}}),$$
$$[\![\mathbf{w}]\!]_e = \mathbf{w}|_{T_{e,1}} - \mathbf{w}|_{T_{e,2}}, \ \{\!\{\mathbf{w}\}\!\}_e = \frac{1}{2}(\mathbf{w}|_{T_{e,1}} + \mathbf{w}|_{T_{e,2}}).$$

For each boundary edge $e \in \mathcal{E}_h^b$, the normal $\mathbf{n}_e$ is the unit outward normal vector. The definitions of the jump and the average are carried over as follows

(3)
$$[\![w]\!]_e = \{\!\{w\}\!\}_e = w, \ [\![\mathbf{w}]\!]_e = \{\!\{\mathbf{w}\}\!\}_e = \mathbf{w}, \ \forall \ e \in \mathcal{E}_h^b.$$

For simplicity, we sometimes omit the subscript from the notations of jump and average if there were no confusion on where these jump and average are defined. For each interface element $T \in \mathcal{T}_h^i$, we denote $\gamma_T = \Gamma \cap T$. The collection of these curved segments of the interface Γ is denoted by $\mathcal{F}_h^i = \{\gamma_T : T \in \mathcal{T}_h^i\}$. The union of interface edges and interface segments in denoted by $\mathcal{M}_h^i = \mathcal{E}_h^i \cup \mathcal{F}_h^i$.

On a subdomain $\tilde{\Omega} \subset \Omega$, let $W^{k,p}(\tilde{\Omega})$ be the standard Sobolev space with the associated norm denoted by $\|\cdot\|_{W^{k,p}(\tilde{\Omega})}$. If $\tilde{\Omega} \cap \Gamma \neq \emptyset$, we denote $\tilde{\Omega}^s := \tilde{\Omega} \cap \Omega^s, s = +, -$. The broken Sobolev spaces on $\tilde{\Omega}$ for $k \geq 2$ are defined by

$$(4) \qquad PW^{k,p}(\tilde{\Omega}) \;=\; \{v \in W^{1,p}(\tilde{\Omega}) : v|_{\tilde{\Omega}^{\pm}} \in [W^{k,p}(\tilde{\Omega}^{\pm})]\},$$

$$(5) \qquad \mathbf{PW}^{k,p}(\tilde{\Omega}) \;=\; \{\mathbf{v} \in [W^{1,p}(\tilde{\Omega})]^2 : \mathbf{v}|_{\tilde{\Omega}^{\pm}} \in [W^{k,p}(\tilde{\Omega}^{\pm})]^2\},$$

equipped the norms

$$(6)$$
$$\|v\|^p_{PW^{k,p}(\tilde{\Omega})} = \|v\|^p_{W^{k,p}(\tilde{\Omega}^+)} + \|v\|^p_{W^{k,p}(\tilde{\Omega}^-)}, \quad \|\mathbf{v}\|^p_{\mathbf{PW}^{k,p}(\tilde{\Omega})} = \|\mathbf{v}\|^p_{\mathbf{W}^{k,p}(\tilde{\Omega}^+)} + \|\mathbf{v}\|^p_{\mathbf{W}^{k,p}(\tilde{\Omega}^-)}.$$

When $p = 2$, the spaces $PW^{k,2}(\tilde{\Omega})$ and $\mathbf{PW}^{k,2}(\tilde{\Omega})$ are simplified to be $PH^k(\tilde{\Omega})$ and $\mathbf{PH}^k(\tilde{\Omega})$, respectively. Moreover, we define the following space that incorporates the Stokes interface jump conditions (1f) - (1g)

$$(7) \qquad \mathcal{U}(\tilde{\Omega}) = \{(\mathbf{v}, q) \in \mathbf{PH}^2(\tilde{\Omega}) \times PH^1(\tilde{\Omega}) : \; [\![\mathbf{v}]\!]_{\Gamma \cap \tilde{\Omega}} = \mathbf{0}, \; [\![\sigma(\mathbf{v}, q)\mathbf{n}]\!]_{\Gamma \cap \tilde{\Omega}} = \mathbf{0}\}.$$

When $\tilde{\Omega} = \Omega$, we define a subspace of $\mathcal{U}(\Omega)$ by

$$(8) \qquad \mathring{\mathcal{U}}(\Omega) = \{(\mathbf{v}, q) \in \mathcal{U}(\Omega) : \int_{\Omega} q d\mathbf{x} = 0\}.$$

2.2. Fictitious Elements. The extension of $\mathcal{P}_k$-$\mathcal{P}_{k-1}$ Taylor-Hood FEM to interface elements requires the construction of high-order IFE shape functions. Unlike the low-order IFE approximations, such as $\mathcal{P}_1$ or $\mathcal{Q}_1$ elements, the higher-order IFE approximation is more sensitive to the relative location of the interface within an element, meaning the interface cannot be too close to a vertex or one piece cannot be too small comparing to the other piece; otherwise the linear system for determining the coefficient of the shape functions will be ill-conditioned. This phenomenon has been reported in [1, 6, 17, 47, 49] for elliptic equations. An effective remedy is to enlarge the physical interface element and construct the IFE shape function on the new fictitious element, as shown in Figure 2. We adopt the fictitious element idea in the construction of Stokes IFE functions.
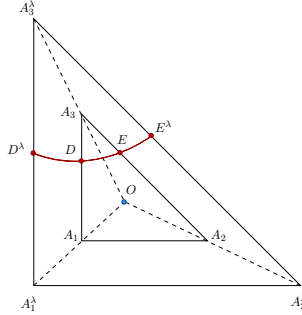

FIGURE 2. An illustration of a fictitious element.

Given a bounded connected subset $K \subset \mathbb{R}^2$, we let

$$K_\lambda = \{X \in \mathbb{R}^2 : \exists \, Y \in K \; \text{such that} \; \overrightarrow{OX} = (1 + \lambda)\overrightarrow{OY}\}$$

be the homothetic image of K with respect to the homothetic center O and the scaling constant λ. For each triangular interface element $T \in \mathcal{T}_h^i$, we set this homothetic center to be its centroid and denote the homothetic image of element T with respect to centroid with a scaling factor λ as T_λ. Then the extended interface segment is denoted by $\gamma_T^\lambda = \Gamma \cap T_\lambda$. We will use this fictitious element T_λ to generate IFE basis functions. See Figure 2 for an illustration, in which $\triangle A_1 A_2 A_3$ is a regular triangle element, and $\triangle A_1^\lambda A_2^\lambda A_3^\lambda$ is the fictitious element. The curve $\widetilde{DE}$ is γ_T, and curve $\widetilde{D^\lambda E^\lambda}$ is γ_T^λ in this case. Furthermore, we state two additional assumptions for the mesh $\mathcal{T}_h$:

   (H4) The mesh is generated such that the interface can only intersect each interface element $T \in \mathcal{T}_h^i$ and its fictitious element T_λ at two distinct points which locate on two different edges of T and T_λ.

   (H5) There exists a fixed integer N such that for each $K \in \mathcal{T}_h$, the number of elements in the set $\{T \in \mathcal{T}_h^i : K \cap T_\lambda \neq \emptyset\}$ is bounded by N.

It has been shown that the smaller subelement of a fictitious element will not be too small and the ratio over the larger subelement is bounded below by some positive constant. More precisely, the following lemma holds.

Lemma 2.1. [49] *For a mesh fine enough and a generic interface curve, given any interface element T and its fictitious element T_λ, $\lambda \leq 1.5$, there exists a positive constant C independent of the interface location such that*

$$(9) \qquad\qquad r(T_\lambda) \geq \frac{4\lambda^2}{9(1+\lambda)^2} - Ch$$

where $r(T_\lambda) = \min\limits_{s=+,-} \{|T_\lambda^s|/|T_\lambda|\}$ with $T_\lambda^s = T_\lambda \cap \Omega^s$.

This feature enables us to construct the high-order IFE shape functions on each fictitious element T_λ instead of the physical interface element $T \in \mathcal{T}_h^i$. More discussion and comparisons will be provided in Section 4.

2.3. Least-Squares $\mathcal{P}_2$-$\mathcal{P}_1$ IFE Functions. In this subsection, we construct the IFE basis functions for the Stokes interface problem (1). The construction is performed on the fictitious element as described above. Let $T \in \mathcal{T}_h$ be a triangular element with the vertices A_1, A_2, A_3. Denote the midpoints of three edges of T by A_4, A_5, and A_6.

First, we recall the standard $\mathcal{P}_2$-$\mathcal{P}_1$ Lagrange vector-valued shape functions. Let $\lambda_{i,T}$ be the barycentric coordinate of triangle T such that $\lambda_{i,T}(A_j) = \delta_{ij}$, $i, j = 1, 2, 3$ where δ_{ij} is the Kronecker delta function. Let $\psi_{i,T}$ be the quadratic Lagrange nodal basis functions on T such that $\psi_{i,T}(A_j) = \delta_{ij}$, $i, j = 1, \cdots, 6$. Then the vector-valued $\mathcal{P}_2$-$\mathcal{P}_1$ Taylor-Hood finite element shape functions $\boldsymbol{\psi}_{i,T}$, $1 \leq i \leq 15$ can be written as

$$(10) \qquad \boldsymbol{\psi}_{i,T} = \begin{pmatrix} \psi_{i,T} \\ 0 \\ 0 \end{pmatrix}, \ 1 \leq i \leq 6, \ \boldsymbol{\psi}_{i,T} = \begin{pmatrix} 0 \\ \psi_{i-6,T} \\ 0 \end{pmatrix}, \ 7 \leq i \leq 12,$$

and

$$(11) \qquad\qquad \boldsymbol{\psi}_{i,T} = \begin{pmatrix} 0 \\ 0 \\ \lambda_{i-12,T} \end{pmatrix}, \ 13 \leq i \leq 15.$$

To simplify the notations for further discussion, we define the nodes N_j, $1 \le j \le 15$ counting multiplicity as follows

$$N_j = A_j, \ \forall \ 1 \le j \le 6, \ N_j = A_{j-6}, \ \forall \ 7 \le j \le 12, \ N_j = A_{j-12}, \ \forall \ 13 \le j \le 15.$$

It can be easily verified that for $1 \le i \le 15$:

(12)
$$\boldsymbol{\psi}_{i,T}(N_j) = (\delta_{ij}, 0, 0), \ 1 \le j \le 6,$$
$$\boldsymbol{\psi}_{i,T}(N_j) = (0, \delta_{ij}, 0), \ 7 \le j \le 12,$$
$$\boldsymbol{\psi}_{i,T}(N_j) = (0, 0, \delta_{ij}), \ 13 \le j \le 15.$$

Let $\mathcal{I} = \{1, 2, \cdots, 15\}$ be the index set, and define the polynomial space $\mathcal{P}(T) :=$ $[\mathbb{P}_2(T)]^2 \times \mathbb{P}_1(T)$. The vector-value finite element space $\mathcal{P}(T)$ can also be written as

(13)
$$\mathcal{P}(T) = \mathrm{span}\{\boldsymbol{\psi}_{i,T} : \ i \in \mathcal{I}\}.$$

Now we construct the IFE function space on each interface triangle $T \in \mathcal{T}_h^i$ where $T^+ := T \cap \Omega^+$ and $T^- := T \cap \Omega^-$. The vector-valued IFE space is a subspace of

(14)
$$\tilde{\mathcal{P}}(T) = \left\{ (\boldsymbol{v}, q) : (\boldsymbol{v}, q)|_{T^+} \in \mathcal{P}(T^+) \text{ and } (\boldsymbol{v}, q)|_{T^-} \in \mathcal{P}(T^-) \right\}$$

which incorporates the interface jump conditions (1f) - (1g). To do this, we split the index set $\mathcal{I}$ into $\mathcal{I}^+ := \{i \in \mathcal{I}, N_i \in T^+\}$ and $\mathcal{I}^- := \{i \in \mathcal{I}, N_i \in T^-\}$. Define the tensor product space $\mathcal{S}(T) := \mathcal{P}(T) \times \mathcal{P}(T)$ and its basis functions $\boldsymbol{\xi}_{i,T}$, $\boldsymbol{\eta}_{i,T}$ where

(15)
$$\boldsymbol{\xi}_{i,T} = \begin{cases} (\boldsymbol{\psi}_{i,T}, \mathbf{0}), & \text{if } i \in \mathcal{I}^+ \\ (\mathbf{0}, \boldsymbol{\psi}_{i,T}), & \text{if } i \in \mathcal{I}^-, \end{cases} \qquad \boldsymbol{\eta}_{i,T} = \begin{cases} (\mathbf{0}, \boldsymbol{\psi}_{i,T}), & \text{if } i \in \mathcal{I}^+, \\ (\boldsymbol{\psi}_{i,T}, \mathbf{0}), & \text{if } i \in \mathcal{I}^-. \end{cases}$$

Apparently, the piecewise polynomial space $\tilde{\mathcal{P}}(T)$ is isomorphic to the tensor-product space $\mathcal{S}(T)$ due to the following one-to-one mapping $\mathcal{H}_T : \mathcal{S}(T) \mapsto \tilde{\mathcal{P}}(T)$:

(16)
$$\mathcal{H}_T(\boldsymbol{w}_1, \boldsymbol{w}_2) = \begin{cases} \boldsymbol{w}_1, & \text{on } T^+ \\ \boldsymbol{w}_2, & \text{on } T^-, \end{cases} \quad \forall (\boldsymbol{w}_1, \boldsymbol{w}_2) \in \mathcal{S}(T).$$

Then we let $\mathcal{V}_1 = \mathrm{span}\{\boldsymbol{\xi}_{i,T}, i \in \mathcal{I}\}$, $\mathcal{V}_2 = \mathrm{span}\{\boldsymbol{\eta}_{i,T}, i \in \mathcal{I}\}$. The tensor product function $\boldsymbol{\phi}_T \in \mathcal{S}(T)$ can be written as

(17)
$$\boldsymbol{\phi}_T = \sum_{i \in \mathcal{I}} v_i \boldsymbol{\xi}_{i,T} + \sum_{i \in \mathcal{I}} c_i \boldsymbol{\eta}_{i,T}$$

where v_i is nodal value at N_i, $i \in \mathcal{I}$. It is easy to see the shape function (17) is constructed by two parts: $\boldsymbol{\xi}_{i,T}$ contribute to nodal values, and $\boldsymbol{\eta}_{i,T}$ are constructed to fit interface conditions as we state in the following.

We enforce the interface conditions in constructing our local IFE shape function in a weak sense. Define a bilinear functional $\mathcal{J}_\lambda : \mathcal{S}(T) \times \mathcal{S}(T) \to \mathbb{R}$ to measure local basis function's fitness of Stokes interface condition as follows

(18)
$$\mathcal{J}_\lambda((\mathbf{u}, p), (\mathbf{v}, q)) = \omega_0 \int_{\gamma_T^\lambda} [\![\mathbf{u}]\!] \, [\![\mathbf{v}]\!] \, ds + \omega_1 h^2 \int_{\gamma_T^\lambda} [\![\nabla \cdot \mathbf{u}]\!] \, [\![\nabla \cdot \mathbf{v}]\!] \, ds$$

$$+ \omega_2 h^2 \int_{\gamma_T^\lambda} [\![\sigma(\mathbf{u}, p)\mathbf{n}]\!] \, [\![\sigma(\mathbf{v}, q)\mathbf{n}]\!] \, ds$$

$$+ \omega_3 h^4 \int_{\gamma_T^\lambda} [\![\nabla \cdot \sigma(\mathbf{u}, p)]\!] \, [\![\nabla \cdot \sigma(\mathbf{v}, q)]\!] \, ds + \omega_4 h^2 \int_{\gamma_T^\lambda} [\![p]\!] \, [\![q]\!] \, ds.$$

Here, $\omega_i > 0$, $i = 0, 1, 2, 3, 4$ are weights of the least-squares functional. The scaling factor h in each term is to balance these weights. It can be seen that the bilinear form $\mathcal{J}_\lambda$ is symmetric and positive semi-definite. We define $|\phi|_{\mathcal{J}_\lambda} = \sqrt{\mathcal{J}_\lambda(\phi, \phi)}$ to be a semi-norm on $\mathcal{S}(T)$.

We consider function space

$$
(19) \qquad \mathcal{V}_2^\perp = \{(\mathbf{u}, p) \in \mathcal{S}(T), \ \mathcal{J}_\lambda((\mathbf{u}, p), (\mathbf{v}, q)) = 0, \ \forall (\mathbf{v}, q) \in \mathcal{V}_2\}
$$

which is the orthogonal complement of $\mathcal{V}_2$ in sense of $\mathcal{J}_\lambda$. Elements in $\mathcal{V}_2^\perp$ are enforced with interface conditions in the least-squares sense.

Following this idea, the calculation of the unknown vector $\mathbf{c} = (c_1, c_2, \cdots, c_{|\mathcal{I}|})$ is by expressing every $\phi_T \in \mathcal{S}(T)$ in the form of (17), then we obtain a linear system for solving $\mathbf{c}$ by the definition of $\mathcal{V}_2^\perp$:

$$
(20) \qquad\qquad \mathbf{Ac} = -\mathbf{Bv}
$$

where
(21)
$$
\mathbf{A}_{ij} = (\mathcal{J}_\lambda (\boldsymbol{\eta}_{j,T}, \boldsymbol{\eta}_{i,T}))_{i,j \in \mathcal{I}} \in \mathbb{R}^{|\mathcal{I}| \times |\mathcal{I}|}, \ \mathbf{B}_{ij} = (\mathcal{J}_\lambda (\boldsymbol{\xi}_{j,T}, \boldsymbol{\eta}_{i,T}))_{i,j \in \mathcal{I}} \in \mathbb{R}^{|\mathcal{I}| \times |\mathcal{I}|}.
$$

Finally, we construct the Lagrange IFE local basis functions $\phi_{i,T}$, $i \in \mathcal{I}$ on $T \in \mathcal{T}_h^i$ by letting $\mathbf{v}$ be the the canonical vector $\mathbf{e}_i$, $1 \le i \le |\mathcal{I}|$:

$$
(22) \qquad\qquad \phi_{i,T} = \mathcal{H}_T(\phi_T|_{\mathbf{e}_i, \mathbf{c}_i}),
$$

here $\mathbf{c}_i$ is solved by $\mathbf{Ac}_i = -\mathbf{Be}_i$.

A comparison of a standard $\mathcal{P}_2$-$\mathcal{P}_1$ Taylor-Hood finite element shape function $\boldsymbol{\psi}_{3,T}$ and our $\mathcal{P}_2$-$\mathcal{P}_1$ IFE shape function $\phi_{3,T}$ is provided in Figure 3. We can see that the second velocity component and the pressure component of the IFE basis function are not entirely zero as in the standard Taylor-Hood basis. This is due to the stress jump condition (1g) in which the velocity and pressure terms are coupled together. Similar features have been observed in other vector-valued IFE functions for Stokes equation [4, 29, 30] and the elasticity equation [19, 38]. Moreover, we notice that the IFE basis functions are generally discontinuous even though each shape function is constructed to satisfy the continuous jump conditions in the least-squares sense [6].

The local FE/IFE space on $T \in \mathcal{T}_h$ can be formed as

$$
(23) \qquad\qquad \mathbf{S}_h(T) = \begin{cases} \text{span}\{\boldsymbol{\psi}_{i,T}, i \in \mathcal{I}\} \text{ if } T \in \mathcal{T}_h^n, \\ \text{span}\{\phi_{i,T}, i \in \mathcal{I}\} \text{ if } T \in \mathcal{T}_h^i. \end{cases}
$$

The global IFE space $\mathbf{S}_h(\Omega)$ is defined by
(24)
$$
\mathbf{S}_h(\Omega) = \left\{ (\mathbf{u}, p) \in [L^2(\Omega)]^3 : \ (\mathbf{u}, p) \text{ satisfies the following conditions (C1)-(C4)} \right\}.
$$
    (C1): $(\mathbf{u}, p)|_T \in \mathbf{S}_h(T)$, for all $T \in \mathcal{T}_h$.
    (C2): $(\mathbf{u}, p)$ is continuous on every non-interface edge $e \in \mathcal{E}_h^n$.
    (C3): $\mathbf{u}$ is continuous at all vertices and midpoints of $T \in \mathcal{T}_h$.
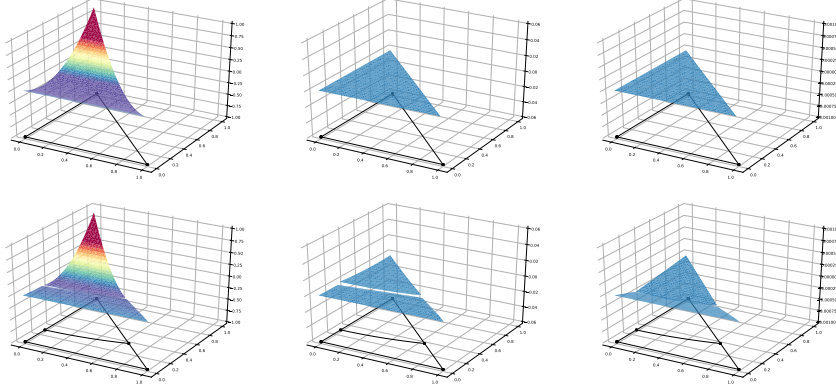   **(C4):** p is continuous at all vertices of $T \in \mathcal{T}_h$.

FIGURE 3. Top (from left): Standard FE shape function $\boldsymbol{\psi}_{3,T}$ for u_1, u_2 and p. Bottom (from left): the IFE shape function $\boldsymbol{\phi}_{3,T}$ for u_1, u_2 and p with the coefficients $(\mu^+, \mu^-) = (10, 1)$.

Then local interpolation operator $I_{h,T} : \mathcal{U}(T) \mapsto \mathbf{S}_h(T)$ is defined by:

$$(25) \quad I_{h,T}(\mathbf{u}, p) = \sum_{i=1}^{6} u_1(N_i) \boldsymbol{\psi}_{i,T} + \sum_{i=7}^{12} u_2(N_i) \boldsymbol{\psi}_{i,T} + \sum_{i=13}^{15} p(N_i) \boldsymbol{\psi}_{i,T}, \text{ if } T \in \mathcal{T}_h^n,$$

$$(26) \quad I_{h,T}(\mathbf{u}, p) = \sum_{i=1}^{6} u_1(N_i) \boldsymbol{\phi}_{i,T} + \sum_{i=7}^{12} u_2(N_i) \boldsymbol{\phi}_{i,T} + \sum_{i=13}^{15} p(N_i) \boldsymbol{\phi}_{i,T}, \text{ if } T \in \mathcal{T}_h^i.$$

The global interpolation operator $I_h : \mathcal{U}(\Omega) \mapsto \mathbf{S}_h(\Omega)$ is:

$$(27) \qquad\qquad I_h(\mathbf{u}, p)|_T = I_{h,T}(\mathbf{u}, p), \ \forall \ T \in \mathcal{T}_h.$$

2.4. Properties of IFE Spaces. In this section, we introduce some properties of the new IFE space. First we prove the existence of the IFE function for any configuration of interface location and coefficients.

Theorem 2.1 (Existence of IFE Function). *On each interface element $T \in \mathcal{T}_h^i$, there exists at least one solution to the linear system* (20).

Proof. To prove the linear system (20) has at least a solution is equivalent to prove $\mathrm{Ker}(\mathbf{A}) \subseteq \mathrm{Ker}(\mathbf{B})$. This is to say $\mathbf{Bm} = \mathbf{0}$ whenever $\mathbf{Am} = \mathbf{0}$ for any vector $\mathbf{v}$. Suppose this is not true, then there exists a vector $\mathbf{m_0}$ such that $\mathbf{Am_0} = \mathbf{0}$ but $\mathbf{Bm_0} \neq \mathbf{0}$. Let $\mathbf{n_0}$ to be a vector such that $\mathbf{n_0}^T \mathbf{Bm_0} < 0$, set $\boldsymbol{\phi}_{\mathbf{0},T} = \phi|_{\epsilon \mathbf{n_0}, \mathbf{m_0}}$ where ϵ is a constant larger than 0. We have

$$(28) \quad \begin{aligned} \mathcal{J}_\lambda(\boldsymbol{\phi}_{\mathbf{0},T}, \boldsymbol{\phi}_{\mathbf{0},T}) &= (\epsilon \mathbf{n_0})^T \mathbf{C}(\epsilon \mathbf{n_0}) + 2(\epsilon \mathbf{n_0})^T \mathbf{Bm_0} + \mathbf{m_0}^T \mathbf{Am_0} \\ &= \epsilon^2 \mathbf{n_0}^T \mathbf{Cn_0} + 2\epsilon \mathbf{n_0}^T \mathbf{Bm_0}. \end{aligned}$$

Here $\mathbf{C}_{ij} = (\mathcal{J}_\lambda(\boldsymbol{\xi}_{i,T}, \boldsymbol{\xi}_{j,T}))_{i,j \in \mathcal{I}} \in \mathbb{R}^{|\mathcal{I}| \times |\mathcal{I}|}$. Let $\epsilon < -2\mathbf{n_0}^T \mathbf{Bm_0} / \mathbf{n_0}^T \mathbf{Cn_0}$, then we obtain $\mathcal{J}_\lambda(\boldsymbol{\phi}_{\mathbf{0},T}, \boldsymbol{\phi}_{\mathbf{0},T}) < 0$ which contradicts with the semi-positive definiteness of $\mathcal{J}_\lambda(\cdot, \cdot)$. $\square$

Theorem 2.2 (Least-Squares Best Approximation). *On each interface element $T \in \mathcal{T}_h^i$, the local IFE function $\boldsymbol{\phi}_T = \boldsymbol{\xi}_T + \boldsymbol{\eta}_T$ minimizes the least squares functional (18), i.e.,*

$$(29) \qquad |\boldsymbol{\xi}_T + \boldsymbol{\eta}_T|_{\mathcal{J}_\lambda} = \min_{\boldsymbol{\zeta}_T \in \mathcal{V}_2} |\boldsymbol{\xi}_T + \boldsymbol{\zeta}_T|_{\mathcal{J}_\lambda}.$$

Proof. Note that every local IFE function can be written as following form:

$$(30) \qquad \boldsymbol{\phi}_T = \boldsymbol{\xi}_T + \boldsymbol{\zeta}_T$$

where $\boldsymbol{\xi}_T \in \mathcal{V}_1$, $\boldsymbol{\zeta}_T \in \mathcal{V}_2$. Then following a standard procedure, we have

$$(31) \qquad \begin{aligned} & |\boldsymbol{\xi}_T + \boldsymbol{\zeta}_T|^2_{\mathcal{J}_\lambda} - |\boldsymbol{\xi}_T + \boldsymbol{\eta}_T|^2_{\mathcal{J}_\lambda} \\ =& |\boldsymbol{\xi}_T + \boldsymbol{\zeta}_T + \boldsymbol{\eta}_T - \boldsymbol{\eta}_T|^2_{\mathcal{J}_\lambda} - |\boldsymbol{\xi}_T + \boldsymbol{\eta}_T|^2_{\mathcal{J}_\lambda} \\ =& |\boldsymbol{\zeta}_T - \boldsymbol{\eta}_T|^2_{\mathcal{J}_\lambda} + 2\mathcal{J}_\lambda(\boldsymbol{\xi}_T + \boldsymbol{\eta}_T, \boldsymbol{\zeta}_T - \boldsymbol{\eta}_T). \end{aligned}$$

Since $\boldsymbol{\zeta}_T - \boldsymbol{\eta}_T \in \mathcal{V}_2$, $\boldsymbol{\xi}_T + \boldsymbol{\eta}_T \in \mathcal{V}_2^\perp$, so $\mathcal{J}_\lambda(\boldsymbol{\xi}_T + \boldsymbol{\eta}_T, \boldsymbol{\zeta}_T - \boldsymbol{\eta}_T) = 0$. So we obtain

$$(32) \qquad |\boldsymbol{\xi}_T + \boldsymbol{\zeta}_T|^2_{\mathcal{J}_\lambda} - |\boldsymbol{\xi}_T + \boldsymbol{\eta}_T|^2_{\mathcal{J}_\lambda} = |\boldsymbol{\zeta}_T - \boldsymbol{\eta}_T|^2_{\mathcal{J}_\lambda} \geq 0.$$

$\square$

The above theorem shows that our choice of $\mathbf{c}$ is the optimal choice for $|\boldsymbol{\phi}_T|_{\mathcal{J}_\lambda}$ for given nodal values $\mathbf{v}$, gauged by the semi-norm $|\cdot|_{\mathcal{J}_\lambda}$ that measures the fitness of interface conditions.

The approximation capability of the new IFE space is investigated numerically in Section 4 through the interpolation error analysis. Let

$$u_{I,1} = (I_h(\mathbf{u}, p))_1, \ \ u_{I,2} = (I_h(\mathbf{u}, p))_2, \ \ p_I = (I_h(\mathbf{u}, p))_3.$$

We observe that the interpolation errors obey

$$(33) \qquad ||u_{I,k} - u_k||_{L^2(\Omega)} + h|u_{I,k} - u_k|_{H^1(\Omega)} \leq \mathcal{O}(h^3), \ \ k = 1, 2,$$

and

$$(34) \qquad ||p_I - p||_{L^2(\Omega)} + h|p_I - p|_{H^1(\Omega)} \leq \mathcal{O}(h^2).$$

3. PPIFEM with Ghost Penalty

We propose the partially penalized IFE method with ghost penalty for Stokes interface problem as follows. Find $(\mathbf{u}_h, p_h) \in \mathbf{S}_h(\Omega)$ such that

$$(35) \qquad \begin{cases} A(\mathbf{u}_h, \mathbf{v}_h) + B(\mathbf{v}_h, p_h) + J_{\mathbf{u}}(\mathbf{u_h}, \mathbf{v_h}) = L(\mathbf{v}_h), \\ B(\mathbf{u}_h, q_h) - J_p(p_h, q_h) = 0, \end{cases} \qquad \forall (\mathbf{v}_h, q_h) \in \mathbf{S}_h(\Omega),$$

where the bilinear forms $A(\cdot, \cdot)$, $B(\cdot, \cdot)$ and the linear form $L(\cdot)$ are defined by

$$
\begin{aligned}
A(\mathbf{u}, \mathbf{v}) = &\int_\Omega 2\nu\boldsymbol{\epsilon}(\mathbf{u}) : \boldsymbol{\epsilon}(\mathbf{v})d\mathbf{x} - \sum_{e \in \mathcal{E}_h^i} \int_e \{\!\{2\nu\boldsymbol{\epsilon}(\mathbf{u})\mathbf{n}\}\!\} \cdot [\![\mathbf{v}]\!]\, ds \\
&+ \epsilon_0 \sum_{e \in \mathcal{E}_h^i} \int_e \{\!\{2\nu\boldsymbol{\epsilon}(\mathbf{v})\mathbf{n}\}\!\} \cdot [\![\mathbf{u}]\!] \\
&+ \frac{\sigma_e^0}{|e|} \sum_{e \in \mathcal{E}_h^i} \int_e [\![\mathbf{u}]\!] \cdot [\![\mathbf{v}]\!]\, ds - \sum_{T \in \mathcal{T}_h^i} \int_{\gamma_T} \{\!\{2\nu\boldsymbol{\epsilon}(\mathbf{u})\mathbf{n}\}\!\} \cdot [\![\mathbf{v}]\!]\, ds \\
&+ \epsilon_1 \sum_{T \in \mathcal{T}_h^i} \int_{\gamma_T} \{\!\{2\nu\boldsymbol{\epsilon}(\mathbf{v})\mathbf{n}\}\!\} \cdot [\![\mathbf{u}]\!] + \frac{\sigma_e^1}{h_T} \sum_{T \in \mathcal{T}_h^i} \int_{\gamma_T} [\![\mathbf{u}]\!] \cdot [\![\mathbf{v}]\!]\, ds,
\end{aligned}
$$

(36)

$$
B(\mathbf{v}, p) = -\int_\Omega p \nabla \cdot \mathbf{v} d\mathbf{x} + \sum_{e \in \mathcal{E}_h^i} \int_e \{\!\{p\mathbf{n}\}\!\} [\![\mathbf{v}]\!]\, ds + \sum_{T \in \mathcal{T}_h^i} \int_{\gamma_T} \{\!\{p\mathbf{n}\}\!\} [\![\mathbf{v}]\!]\, ds,
$$

$$
L(\mathbf{v}) = \int_\Omega \mathbf{f} \cdot \mathbf{v} d\mathbf{x}.
$$

The ghost penalty terms in (35) are defined as:

(37)

$$
\begin{aligned}
J_\mathbf{u}(\mathbf{u}, \mathbf{v}) &= \sum_{e \in \mathcal{M}_h^i} \sum_{1 \le j \le k} \sigma_{\mathbf{u},j} h_T^{2j-1} \int_e \{\!\{\nu\}\!\} \left[\partial_\mathbf{n}^j \mathbf{u}\right] : \left[\partial_\mathbf{n}^j \mathbf{v}\right] ds, \\
J_p(p, q) &= \sum_{e \in \mathcal{M}_h^i} \sum_{0 \le j \le k} \sigma_{p,j} h_T^{2j+1} \int_e \{\!\{\nu\}\!\}^{-1} \left[\partial_\mathbf{n}^j p\right] \cdot \left[\partial_\mathbf{n}^j q\right] ds.
\end{aligned}
$$

In (36)-(37), σ_e^0, σ_e^1, $\sigma_{\mathbf{u},j}$ and $\sigma_{p,j}$ are penalty parameters. The integer k in ghost penalty terms refers to the order of polynomials (e.g. for the $\mathcal{P}_2$-$\mathcal{P}_1$ element, $k = 2$ in $J_\mathbf{u}$ and $k = 1$ in J_p). The parameter ϵ_0 may take the value -1 or 0 or 1 which refers to the symmetric, incomplete and non-symmetric partially penalized IFEM, respectively [36].

In $A(\mathbf{u}, \mathbf{v})$, we add partially penalized terms on both interface edges and the interface itself. Approximating functions are not guaranteed to be continuous across interface elements. The aim of adding penalty terms is to impose the continuity of approximation and ensure that the coercivity [36]. Several research of IFEM have verified effectiveness of this technique, including immersed DG method for Stokes interface problem [4, 5]. Apart from the edge penalty, we add penalty terms on interface as well, since continuity of basis function inside the element cannot be guaranteed in our least-squares approximation space. This idea has been employed in [1, 6, 17]. In the numerical examples, we take corresponding parameters of penalty on edges same as parameters of penalty on interface. Similar weak forms are also proposed for imposing continuity within the interface elements for high-order PPIFE for the elliptic equations [1, 17].

In our numerical scheme, the ghost penalty terms $J_\mathbf{u}(\mathbf{u}_h, \mathbf{v}_h)$ and $J_p(p_h, q_h)$ are added for stabilization. Similar to partially penalized terms, the objective of adding these terms is to control discontinuous polynomials around the interface. The operators defined in (37) try to minimize the inter-element normal derivative jumps $\partial_\mathbf{n}\mathbf{u}$ and $\partial_\mathbf{n}p$. Different orders are weighted with a proper scaling of h for consistency. Moreover, several methods for Stokes interface problems mention that

$J_p(p_h, q_h)$ is necessary for proving inf-sup stability such as XFEM [32], Nitsche's method [46] and Cut-FEM [14, 24, 41]. The term $J_{\mathbf{u}}(\mathbf{u}_h, \mathbf{v}_h)$ will serve for improving the coercivity when the interface cuts the boundary of the domain [24]. Although the set of edges we stabilize is slightly different from methods above, we believe these terms would achieve similar effect which could be also revealed from our numerical examples in the following section.

4. Numerical Experiments

In this section, we provide three classes of numerical experiments. The first one (Examples 4.1 and 4.2) is a convergence test of both interpolations and IFE solutions in two different interface shapes. The second test (Example 4.3) focuses on the effect of the ghost penalty for IFE schemes. The third test (Example 4.4) demonstrate the advantages of the fictitious element over the actual element when the interface is close to vertices.

In our numerical experiments, we use a family of Cartesian triangular meshes $\{\mathcal{T}_h\}$ of Ω. These meshes are generated by first partitioning Ω into $N \times N$ standard uniform squares, and then each square is further partitioned by its diagonal with negative slope. The mesh size h is defined to be $2/N$. To compute the least-squares IFE basis functions, we set $\omega_0 = \max(\nu^+, \nu^-)$, $\omega_1 = 1$, $\omega_2 = 1$, $\omega_3 = 1$, $\omega_4 = 100\max(\nu^+, \nu^-)$ for weights of bilinear form (18). The interface cut each interface triangle into two curved polygons. Numerical quadratures on curve segments and on curved polygons are performed by a proper mapping into line segment and standard triangles. The numerical quadratures on curves and curved domains has been reported in [3].

Example 4.1. *In this example, we test accuracy and convergence of the PPIFE method with ghost penalty. We first consider the straight line interface* $\Gamma = \{(x, y) \in \Omega : 2x + y - c = 0\}$ *which separates the domain* $\Omega = (-1, 1) \times (-1, 1)$ *into* $\Omega^+ = \{(x, y) \in \Omega : 2x + y - c > 0\}$ *and* $\Omega^- = \{(x, y) \in \Omega : 2x + y - c < 0\}$. *Here we let* $c = \sqrt{2}$. *The exact solution* $\mathbf{u}$ *and* p *are defined as follows*

$$\mathbf{u} = \begin{cases} \begin{pmatrix} (2x + y - c)^3/(2\nu^+) \\ -(2x + y - c)^3/\nu^+ \end{pmatrix}, & in\ \Omega^+, \\ \begin{pmatrix} (2x + y - c)^3/(2\nu^-) \\ -(2x + y - c)^3/\nu^- \end{pmatrix}, & in\ \Omega^-, \end{cases}$$

and

$$p = e^x - e^y.$$

The interpolation error is shown in Tables 1 and 2. The data obey the expected convergence rates (33)-(34). We also notice that the interpolation functions are identical regardless the coefficient values for $\omega_i, i = 0, 1, 2, 3, 4$ for this linear interface case. For the PPIFE method, we use the symmetric weak formulation. We take $\sigma_e^1 = \sigma_e^0 = 1500$, $\sigma_{u,1} = 0$, $\sigma_{p,0} = \sigma_{p,1} = 1$ in our experiments. Computational results for IFE solutions are listed in Table 3 and 4. We test convergence performance of the IFE method for both small and large jumps, i.e., (ν^+, ν^-) is set to be $(10, 1)$ and $(1000, 1)$, respectively. All data indicate that IFE solutions obey

(38) $$\|u_{h,k} - u_k\|_{L^2(\Omega)} + h|u_{h,k} - u_k|_{H^1(\Omega)} \leq \mathcal{O}(h^3),\ k = 1, 2,$$

and

(39) $$\|p_h - p\|_{L^2(\Omega)} + h|p_h - p|_{H^1(\Omega)} \leq \mathcal{O}(h^2).$$

An illustration of IFE solution with both jumps is given in Figure 4. In the diagrams, the background is a contour plot of pressure values. The stream lines are curves tangent to the velocity vector, the line thickness reflects the magnitude of velocity vectors.

TABLE 1. Interpolation error of Example 4.1 with $(10, 1)$ at $\lambda = 1.0$.

λ	N	$\|u_{I,1} - u_1\|_{L^2}$	order	$\|u_{I,2} - u_2\|_{L^2}$	order	$\|p_I - p\|_{L^2}$	order
	10	9.15×10^{-4}		1.83×10^{-3}		8.36×10^{-3}	
	20	1.14×10^{-4}	3.00	2.28×10^{-4}	3.00	2.10×10^{-3}	1.99
	40	1.43×10^{-5}	2.99	2.85×10^{-5}	3.00	5.25×10^{-4}	2.00
	80	1.79×10^{-6}	3.00	3.57×10^{-6}	3.00	1.31×10^{-4}	2.00
	160	2.23×10^{-7}	3.00	4.47×10^{-7}	3.00	3.28×10^{-5}	2.00
1.0	N	$\|u_{I,1} - u_1\|_{H^1}$	order	$\|u_{I,2} - u_2\|_{H^1}$	order	$\|p_I - p\|_{H^1}$	order
	10	4.84×10^{-2}		9.68×10^{-2}		2.19×10^{-1}	
	20	1.21×10^{-2}	2.00	2.42×10^{-2}	2.00	1.10×10^{-1}	0.99
	40	3.03×10^{-3}	2.00	6.06×10^{-3}	2.00	5.50×10^{-2}	1.00
	80	7.59×10^{-4}	2.00	1.52×10^{-3}	2.00	2.75×10^{-2}	1.00
	160	1.90×10^{-4}	2.00	3.80×10^{-4}	2.00	1.37×10^{-2}	1.01

TABLE 2. Interpolation error of Example 4.1 with $(1000, 1)$ at $\lambda = 1.0$.

λ	N	$\|u_{I,1} - u_1\|_{L^2}$	order	$\|u_{I,2} - u_2\|_{L^2}$	order	$\|p_I - p\|_{L^2}$	order
	10	9.06×10^{-4}		1.81×10^{-3}		8.36×10^{-3}	
	20	1.14×10^{-4}	2.99	2.27×10^{-4}	3.00	2.10×10^{-3}	1.99
	40	1.42×10^{-5}	3.01	2.85×10^{-5}	2.99	5.25×10^{-4}	2.00
	80	1.78×10^{-6}	3.00	3.57×10^{-6}	3.00	1.31×10^{-4}	2.00
	160	2.23×10^{-7}	3.00	4.46×10^{-7}	3.00	3.28×10^{-5}	2.00
1.0	N	$\|u_{I,1} - u_1\|_{H^1}$	order	$\|u_{I,2} - u_2\|_{H^1}$	order	$\|p_I - p\|_{H^1}$	order
	10	4.82×10^{-2}		9.64×10^{-2}		2.19×10^{-1}	
	20	1.21×10^{-2}	1.99	2.42×10^{-2}	1.99	1.10×10^{-1}	0.99
	40	3.03×10^{-3}	2.00	6.05×10^{-3}	2.00	5.50×10^{-2}	1.00
	80	7.58×10^{-4}	2.00	1.52×10^{-3}	1.99	2.75×10^{-2}	1.00
	160	1.90×10^{-4}	2.00	3.79×10^{-4}	2.00	1.37×10^{-2}	1.01

Example 4.2. *In this example, we test a curved interface, which has been used in [4, 29, 30]. The domain $\Omega = (-1, 1)^2$ is split into Ω^+ and Ω^- by circular interface $\Gamma = \{(x,y) \in \Omega : x^2 + y^2 - r^2 = 0\}$, where $\Omega^+ = \{(x,y) \in \Omega : x^2 + y^2 - r^2 > 0\}$ and $\Omega^- = \{(x,y) \in \Omega : x^2 + y^2 - r^2 < 0\}$ with $r^2 = 0.3$. The exact solution to this Stokes equation is*

$$\mathbf{u} = \begin{cases} \begin{pmatrix} y(x^2 + y^2 - r^2)/\nu^+ \\ -x(x^2 + y^2 - r^2)/\nu^+ \end{pmatrix}, & in\ \Omega^+ \\ \begin{pmatrix} y(x^2 + y^2 - r^2)/\nu^- \\ -x(x^2 + y^2 - r^2)/\nu^- \end{pmatrix}, & in\ \Omega^-, \end{cases}$$

TABLE 3. SPPIFE error of Example 4.1 with $(10, 1)$ at $\lambda = 1.0$.

λ	N	$\|u_{h,1} - u_1\|_{L^2}$	order	$\|u_{h,2} - u_2\|_{L^2}$	order	$\|p_h - p\|_{L^2}$	order
	10	9.64×10^{-4}		1.86×10^{-3}		4.85×10^{-2}	
	20	1.17×10^{-4}	3.04	2.31×10^{-4}	3.01	7.90×10^{-3}	2.62
	40	1.45×10^{-5}	3.01	2.87×10^{-5}	3.01	1.27×10^{-3}	2.64
	80	1.81×10^{-6}	3.00	3.59×10^{-6}	3.00	2.14×10^{-4}	2.57
	160	2.24×10^{-7}	3.01	4.47×10^{-7}	3.01	2.71×10^{-5}	2.98
1.0	N	$|u_{h,1} - u_1|_{H^1}$	order	$|u_{h,2} - u_2|_{H^1}$	order	$|p_h - p|_{H^1}$	order
	10	4.85×10^{-2}		9.66×10^{-2}		8.72×10^{-1}	
	20	1.21×10^{-2}	2.00	2.42×10^{-2}	2.00	2.71×10^{-1}	1.69
	40	3.03×10^{-3}	2.00	6.06×10^{-3}	2.00	9.27×10^{-2}	1.55
	80	7.59×10^{-4}	2.00	1.52×10^{-3}	2.00	3.63×10^{-2}	1.35
	160	1.90×10^{-4}	2.00	3.80×10^{-4}	2.00	1.44×10^{-2}	1.33

TABLE 4. SPPIFE Error of Example 4.1 with $(1000, 1)$ at $\lambda = 1.0$.

| λ	N	$\|u_{h,1} - u_1\|_{L^2}$	order	$\|u_{h,2} - u_2\|_{L^2}$	order	$\|p_h - p\|_{L^2}$	order
	10	9.54×10^{-4}		1.83×10^{-3}		5.73×10^{-2}	
	20	1.16×10^{-4}	3.04	2.29×10^{-4}	3.00	1.13×10^{-2}	2.34
	40	1.44×10^{-5}	3.01	2.86×10^{-5}	3.00	2.19×10^{-3}	2.37
	80	1.79×10^{-6}	3.01	3.58×10^{-6}	3.00	3.18×10^{-4}	2.78
	160	2.23×10^{-7}	3.00	4.46×10^{-7}	3.00	7.19×10^{-5}	2.14
1.0	N	$|u_{h,1} - u_1|_{H^1}$	order	$|u_{h,2} - u_2|_{H^1}$	order	$|p_h - p|_{H^1}$	order
	10	4.83×10^{-2}		9.62×10^{-2}		9.80×10^{-1}	
	20	1.21×10^{-2}	2.00	2.42×10^{-2}	1.99	3.65×10^{-1}	1.42
	40	3.03×10^{-3}	2.00	6.06×10^{-3}	2.00	1.38×10^{-1}	1.40
	80	7.59×10^{-4}	2.00	1.52×10^{-3}	2.00	4.48×10^{-2}	1.62
	160	1.90×10^{-4}	2.00	3.79×10^{-4}	2.00	1.74×10^{-2}	1.36
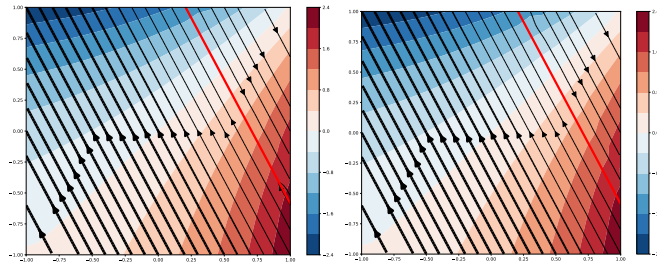
FIGURE 4. Stream Line of Example 2, Left: contrast (10,1), Right: contrast (1000,1).

and

$$p = \frac{1}{10}(x^3 - y^3).$$

We take $\sigma_{u,1} = \sigma_e^1 = \sigma_e^0 = 100$, $\sigma_{p,0} = 1$ and $\sigma_{p,1} = 0$ in the weak form. The IFE solution errors are listed in Table 7 and 8. Similar with linear interface case, both small and large jumps are tested for this interface problem. An illustration of curved interface case numerical results with small and large jump is shown in Figure 5. As before, the interpolation and IFE solution converge optimally in both L^2 and H^1 norms.

TABLE 5. Interpolation error of Example 4.2 with $(10, 1)$ at $\lambda = 1.0$.

λ	N	$\|u_{I,1} - u_1\|_{L^2}$	order	$\|u_{I,2} - u_2\|_{L^2}$	order	$\|p_I - p\|_{L^2}$	order
	10	3.38×10^{-4}		3.38×10^{-4}		3.56×10^{-3}	
	20	3.81×10^{-5}	3.15	3.81×10^{-5}	3.15	8.94×10^{-4}	1.99
	40	4.82×10^{-6}	2.98	4.82×10^{-6}	2.98	2.24×10^{-4}	2.00
	80	5.97×10^{-7}	3.01	5.97×10^{-7}	3.01	5.64×10^{-5}	1.99
	160	7.45×10^{-8}	3.00	7.45×10^{-8}	3.00	1.44×10^{-5}	1.97
1.0	N	$|u_{I,1} - u_1|_{H^1}$	order	$|u_{I,2} - u_2|_{H^1}$	order	$|p_I - p|_{H^1}$	order
	10	1.28×10^{-2}		1.28×10^{-2}		5.63×10^{-2}	
	20	3.08×10^{-3}	2.06	3.08×10^{-3}	2.06	2.83×10^{-2}	0.99
	40	7.65×10^{-4}	2.01	7.65×10^{-4}	2.01	1.42×10^{-2}	0.99
	80	1.91×10^{-4}	2.00	1.91×10^{-4}	2.00	7.15×10^{-3}	0.99
	160	4.81×10^{-5}	1.99	4.81×10^{-5}	1.99	3.66×10^{-3}	0.97

TABLE 6. Interpolation error of Example 4.2 with $(1000, 1)$ at $\lambda = 1.0$.

λ	N	$\|u_{I,1} - u_1\|_{L^2}$	order	$\|u_{I,2} - u_2\|_{L^2}$	order	$\|p_I - p\|_{L^2}$	order
	10	3.27×10^{-4}		3.27×10^{-4}		3.56×10^{-3}	
	20	4.03×10^{-5}	3.02	4.03×10^{-5}	3.02	8.93×10^{-4}	2.00
	40	4.69×10^{-6}	3.10	4.69×10^{-6}	3.10	2.24×10^{-4}	2.00
	80	5.85×10^{-7}	3.00	5.85×10^{-7}	3.00	5.59×10^{-5}	2.00
	160	7.31×10^{-8}	3.00	7.31×10^{-8}	3.00	1.40×10^{-5}	2.00
1.0	N	$|u_{I,1} - u_1|_{H^1}$	order	$|u_{I,2} - u_2|_{H^1}$	order	$|p_I - p|_{H^1}$	order
	10	1.27×10^{-2}		1.27×10^{-2}		5.63×10^{-2}	
	20	3.22×10^{-3}	1.98	3.22×10^{-3}	1.98	2.83×10^{-2}	0.99
	40	7.46×10^{-4}	2.11	7.46×10^{-4}	2.11	1.41×10^{-2}	1.01
	80	1.89×10^{-4}	1.98	1.89×10^{-4}	1.98	7.07×10^{-3}	1.00
	160	4.73×10^{-5}	2.00	4.73×10^{-5}	2.00	3.54×10^{-3}	1.00

Example 4.3. *In this example, we test the effect of the ghost penalty terms to the IFE solution, especially for the pressure. We set the pressure to be 0 (a simpler case than Example 4.1) and test the scheme with and without the ghost penalty. Here we use the straight line interface as in Example 4.1. The exact solution can be written as:*

TABLE 7. SPPIFE error of Example 4.2 with $(10, 1)$ at $\lambda = 1.0$.

λ	N	$\|u_{h,1} - u_1\|_{L^2}$	order	$\|u_{h,2} - u_2\|_{L^2}$	order	$\|p_h - p\|_{L^2}$	order
	10	5.94×10^{-4}		5.94×10^{-4}		3.68×10^{-2}	
	20	5.43×10^{-5}	3.45	5.43×10^{-5}	3.45	4.62×10^{-3}	2.99
	40	6.55×10^{-6}	3.05	6.55×10^{-6}	3.05	8.48×10^{-4}	2.45
	80	6.56×10^{-7}	3.32	6.56×10^{-7}	3.32	1.11×10^{-4}	2.93
	160	7.63×10^{-8}	3.10	7.63×10^{-8}	3.10	1.67×10^{-5}	2.73
1.0	N	$|u_{h,1} - u_1|_{H^1}$	order	$|u_{h,2} - u_2|_{H^1}$	order	$|p_h - p|_{H^1}$	order
	10	1.37×10^{-2}		1.37×10^{-2}		4.47×10^{-1}	
	20	3.18×10^{-3}	2.11	3.18×10^{-3}	2.11	1.39×10^{-1}	1.69
	40	8.15×10^{-4}	1.96	8.15×10^{-4}	1.96	5.67×10^{-2}	1.29
	80	1.94×10^{-4}	2.07	1.94×10^{-4}	2.07	1.50×10^{-2}	1.92
	160	4.78×10^{-5}	2.02	4.78×10^{-5}	2.02	5.21×10^{-3}	1.53

TABLE 8. SPPIFE error of Example 4.2 with $(1000, 1)$ at $\lambda = 1.0$.

| λ	N	$\|u_{h,1} - u_1\|_{L^2}$	order	$\|u_{h,2} - u_2\|_{L^2}$	order	$\|p_h - p\|_{L^2}$	order
	10	8.88×10^{-4}		8.88×10^{-4}		1.48×10^{-1}	
	20	5.19×10^{-5}	4.10	5.19×10^{-5}	4.10	6.31×10^{-2}	1.23
	40	7.81×10^{-6}	2.73	7.81×10^{-6}	2.73	7.98×10^{-3}	2.98
	80	7.28×10^{-7}	3.42	7.28×10^{-7}	3.42	1.43×10^{-3}	2.48
	160	7.78×10^{-8}	3.23	7.78×10^{-8}	3.23	2.82×10^{-4}	2.34
1.0	N	$|u_{h,1} - u_1|_{H^1}$	order	$|u_{h,2} - u_2|_{H^1}$	order	$|p_h - p|_{H^1}$	order
	10	1.63×10^{-2}		1.63×10^{-2}		$2.39 \times 10^{+0}$	
	20	3.35×10^{-3}	2.28	3.35×10^{-3}	2.28	$1.76 \times 10^{+0}$	0.44
	40	9.09×10^{-4}	1.88	9.09×10^{-4}	1.88	4.81×10^{-1}	1.87
	80	2.02×10^{-4}	2.17	2.02×10^{-4}	2.17	2.02×10^{-1}	1.25
	160	4.81×10^{-5}	2.07	4.81×10^{-5}	2.07	7.39×10^{-2}	1.45
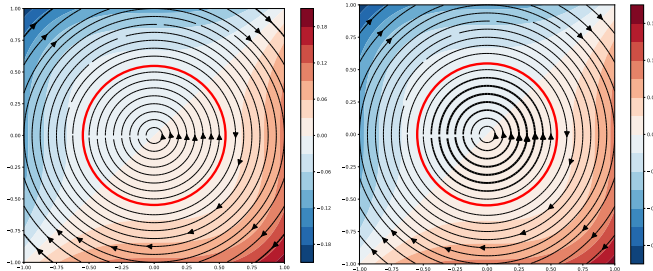
FIGURE 5. Stream Line of Example 1, Left: contrast (10,1), Right: contrast (1000,1).

$$\mathbf{u} = \begin{cases} \begin{pmatrix} (2x + y - c)^3/(2\nu^+) \\ -(2x + y - c)^3/\nu^+ \end{pmatrix}, & \mathbf{x} \in \Omega^+ \\ \begin{pmatrix} (2x + y - c)^3/(2\nu^-) \\ -(2x + y - c)^3/\nu^- \end{pmatrix}, & \mathbf{x} \in \Omega^-, \end{cases}$$

and
$$p = 0.$$
We present symmetric PPIFE results for this example with coefficients $(10, 1)$ and its flipped coefficients $(1, 10)$ in Tables 9, 10, 11 and 12.

TABLE 9. SPPIFE Error of Example 4.3 with $(10, 1)$ at $\lambda = 1.0$ with Ghost Penalty.

λ	N	$\|u_{h,1} - u_1\|_{L^2}$	order	$\|u_{h,2} - u_2\|_{L^2}$	order	$\|p_h - p\|_{L^2}$	order
	10	9.62×10^{-4}		1.84×10^{-3}		3.55×10^{-2}	
	20	1.16×10^{-4}	3.05	2.29×10^{-4}	3.01	4.49×10^{-3}	2.98
	40	1.43×10^{-5}	3.02	2.86×10^{-5}	3.00	5.55×10^{-4}	3.02
	80	1.79×10^{-6}	3.00	3.58×10^{-6}	3.00	6.81×10^{-5}	3.03
	160	2.24×10^{-7}	3.00	4.47×10^{-7}	3.00	9.15×10^{-6}	2.90
λ	N	$|u_{h,1} - u_1|_{H^1}$	order	$|u_{h,2} - u_2|_{H^1}$	order	$|p_h - p|_{H^1}$	order
	10	4.85×10^{-2}		9.66×10^{-2}		7.25×10^{-1}	
1.0	20	1.21×10^{-2}	2.00	2.42×10^{-2}	2.00	1.80×10^{-1}	2.01
	40	3.03×10^{-3}	2.00	6.06×10^{-3}	2.00	4.49×10^{-2}	2.00
	80	7.59×10^{-4}	2.00	1.52×10^{-3}	2.00	1.12×10^{-2}	2.00
	160	1.90×10^{-4}	2.00	3.80×10^{-4}	2.00	2.99×10^{-3}	1.91

TABLE 10. SPPIFE Error of Example 4.3 with $(10, 1)$ at $\lambda = 1.0$ without Ghost Penalty.

λ	N	$\|u_{h,1} - u_1\|_{L^2}$	order	$\|u_{h,2} - u_2\|_{L^2}$	order	$\|p_h - p\|_{L^2}$	order
	10	9.51×10^{-4}		1.85×10^{-3}		4.84×10^{-2}	
	20	1.16×10^{-4}	3.04	2.29×10^{-4}	3.01	6.36×10^{-3}	2.93
	40	1.43×10^{-5}	3.02	2.86×10^{-5}	3.00	7.97×10^{-4}	3.00
	80	1.81×10^{-6}	2.98	3.58×10^{-6}	3.00	4.34×10^{-4}	0.88
	160	2.24×10^{-7}	3.01	4.47×10^{-7}	3.00	2.08×10^{-5}	4.38
λ	N	$|u_{h,1} - u_1|_{H^1}$	order	$|u_{h,2} - u_2|_{H^1}$	order	$|p_h - p|_{H^1}$	order
	10	4.85×10^{-2}		9.66×10^{-2}		9.25×10^{-1}	
1.0	20	1.21×10^{-2}	2.00	2.42×10^{-2}	2.00	2.42×10^{-1}	1.93
	40	3.03×10^{-3}	2.00	6.06×10^{-3}	2.00	6.76×10^{-2}	1.84
	80	7.60×10^{-4}	2.00	1.52×10^{-3}	2.00	9.82×10^{-2}	-0.54
	160	1.90×10^{-4}	2.00	3.80×10^{-4}	2.00	6.43×10^{-3}	3.93

In this simple case $p \equiv 0$, we observed a super-convergence phenomena similar to standard Taylor-Hood finite element method. The IFE scheme without ghost penalty performs unstably. Tables 10 and 12 provide two typical results. In Table 10 with coefficients set to be $(10, 1)$, the convergence seems to be stable on coarse grids, however, it deteriorates as meshes become finer. For coefficients set to be $(1, 10)$ in Table 12, numerical results of pressure are extremely unstable even at coarse meshes.

TABLE 11. SPPIFE Error of Example 4.3 with $(1, 10)$ at $\lambda = 1.0$ with Ghost Penalty.

λ	N	$\|u_{h,1} - u_1\|_{L^2}$	order	$\|u_{h,2} - u_2\|_{L^2}$	order	$\|p_h - p\|_{L^2}$	order
	10	4.90×10^{-4}		8.45×10^{-4}		3.70×10^{-2}	
	20	5.31×10^{-5}	3.21	1.03×10^{-4}	3.04	4.46×10^{-3}	3.05
	40	6.50×10^{-6}	3.03	1.27×10^{-5}	3.02	5.64×10^{-4}	2.98
	80	7.92×10^{-7}	3.04	1.58×10^{-6}	3.01	7.59×10^{-5}	2.89
	160	1.00×10^{-7}	2.99	1.99×10^{-7}	2.99	1.18×10^{-5}	2.69
1.0	N	$|u_{h,1} - u_1|_{H^1}$	order	$|u_{h,2} - u_2|_{H^1}$	order	$|p_h - p|_{H^1}$	order
	10	2.19×10^{-2}		4.26×10^{-2}		7.16×10^{-1}	
	20	5.39×10^{-3}	2.02	1.07×10^{-2}	1.99	1.78×10^{-1}	2.01
	40	1.34×10^{-3}	2.01	2.67×10^{-3}	2.00	4.47×10^{-2}	1.99
	80	3.34×10^{-4}	2.00	6.68×10^{-4}	2.00	1.13×10^{-2}	1.98
	160	8.41×10^{-5}	1.99	1.68×10^{-4}	1.99	3.23×10^{-3}	1.81

TABLE 12. SPPIFE Error of Example 4.3 with $(1, 10)$ at $\lambda = 1.0$ without Ghost Penalty.

λ	N	$\|u_h^1 - u^1\|_{L^2}$	order	$\|u_h^2 - u^2\|_{L^2}$	order	$\|p_h - p\|_{L^2}$	order
	10	5.15×10^{-4}		8.49×10^{-4}		6.02×10^{-2}	
	20	8.67×10^{-4}	-0.75	9.61×10^{-4}	-0.18	3.94×10^{-1}	-2.71
	40	1.01×10^{-5}	6.42	1.50×10^{-5}	6.00	6.05×10^{-3}	6.03
	80	6.22×10^{-6}	0.70	4.66×10^{-6}	1.69	1.04×10^{-2}	-0.78
	160	1.00×10^{-7}	5.96	1.99×10^{-7}	4.55	3.79×10^{-5}	8.10
1.0	N	$|u_{h,1} - u_1|_{H^1}$	order	$|u_{h,2} - u_2|_{H^1}$	order	$|p_h - p|_{H^1}$	order
	10	2.20×10^{-2}		4.24×10^{-2}		$1.35 \times 10^{+0}$	
	20	2.26×10^{-2}	-0.04	3.72×10^{-2}	0.19	$2.19 \times 10^{+1}$	-4.02
	40	1.46×10^{-3}	3.95	2.80×10^{-3}	3.73	6.33×10^{-1}	5.11
	80	1.43×10^{-3}	0.03	1.03×10^{-3}	1.44	$2.62 \times 10^{+0}$	-2.05
	160	8.41×10^{-5}	4.09	1.68×10^{-4}	2.62	1.37×10^{-2}	7.58

Example 4.4. *In this example, we revisit the Example 4.2 to examine the performance of fictitious element mentioned in Section 2.2. A triangular element with the size $h = 0.1$ is intersected by a circular interface with varying radiuses which are illustrated in Figure 6. When the interface intersects elements with small segments, the condition number of $\mathbf{A}$, denoted as $\kappa_{\mathbf{A}}$, blows up, as reported in Table 13. This phenomenon can be alleviated by introducing the fictitious elements, see Table 13 and 14 for comparisons.*

From the results, we find that when the interface segment within an element is small, the magnitude of condition number of $\mathbf{A}$ could be as large as 10^{16} at moderate contrast $(10, 1)$. The magnitude becomes even larger in higher contrast case $(1000, 1)$, which reaches a magnitude of 10^{20}. When we use fictitious elements by setting $\lambda = 0.5, 1.0, 1.5$, the condition number $\kappa_{\mathbf{A}}$ decreases significantly to a
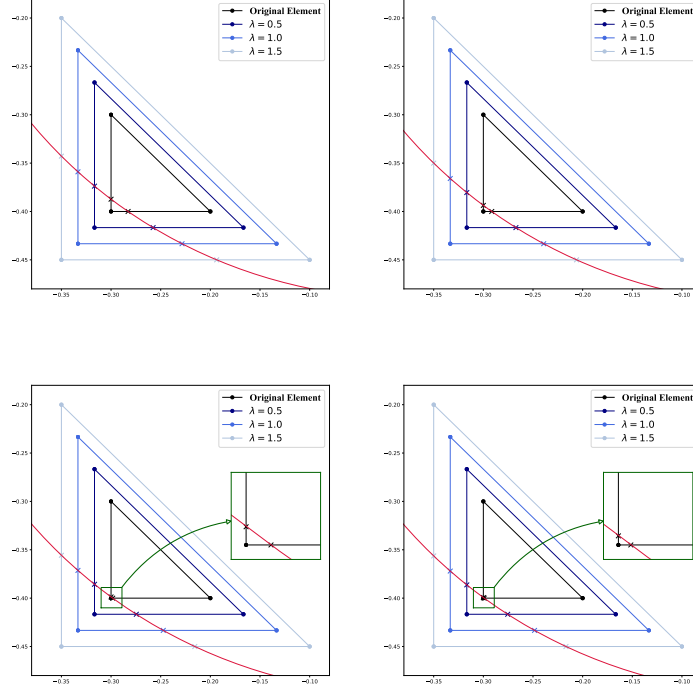
FIGURE 6. From Left to Right: First Line: Elements intersected by circular interface with $r^2 = 0.24, 0.245$, Second Line: Elements intersected by circular interface with $r^2 = 0.249, 0.2495$.

TABLE 13. Condition Numbers for $\mathbf{A}$ with coefficients $(10, 1)$ and varying λ in Example 4.4.

	$\kappa_{\mathbf{A}}$			
	$\lambda = 0$	$\lambda = 0.5$	$\lambda = 1.0$	$\lambda = 1.5$
$r^2 = 0.2400$	5.9227E+10	4.2231E+08	4.1618E+07	8.1810E+06
$r^2 = 0.2450$	1.3704E+12	1.1654E+09	8.7194E+07	1.5400E+07
$r^2 = 0.2490$	1.1470E+15	2.8519E+09	1.6133E+08	2.5920E+07
$r^2 = 0.2495$	1.9027E+16	3.2097E+09	1.7448E+08	2.7679E+07

magnitude of 10^6 when the contrast being $(10, 1)$, and 10^{11} for the contrast being $(1000, 1)$.

5. Conclusion

In this article, we develop a high-order numerical scheme to solve Stokes interface problems on interface-unfitted meshes. An immersed $\mathcal{P}_2$-$\mathcal{P}_1$ Taylor-Hood finite element space is developed based on least square construction on fictitious elements.

TABLE 14. Condition Numbers for **A** with coefficients $(1000, 1)$ and varying λ in Example 4.4.

	$\kappa_{\mathbf{A}}$			
	$\lambda = 0$	$\lambda = 0.5$	$\lambda = 1.0$	$\lambda = 1.5$
$r^2 = 0.2400$	2.2326E+14	1.6353E+12	2.0103E+11	6.4952E+10
$r^2 = 0.2450$	6.2710E+15	5.3336E+12	4.1596E+11	1.0124E+11
$r^2 = 0.2490$	5.9345E+18	1.4701E+13	8.3261E+11	1.5309E+11
$r^2 = 0.2495$	9.9791E+19	1.6768E+13	9.1080E+11	1.6218E+11

The proposed IFE method contains penalties on both interface edges and the actual interface. Ghost penalty terms are also enforced to enhance the stability of the numerical scheme. Numerical results indicate optimal convergence rate of our new IFE method.

6. Acknowledgement

References

[1] Slimane Adjerid, Ivo Babuska, Ruchi Guo, and Tao Lin. An enriched immersed finite element method for interface problems with nonhomogeneous jump conditions. *arXiv preprint arXiv:2004.13244*, 2020.

[2] Slimane Adjerid, Mohamed Ben-Romdhane, and Tao Lin. Higher degree immersed finite element methods for second-order elliptic interface problems. *International Journal of Numerical Analysis & Modeling*, 11(3):541–566, 2014.

[3] Slimane Adjerid, Mohamed Ben-Romdhane, and Tao Lin. Higher degree immersed finite element spaces constructed according to the actual interface. *Computers & Mathematics with Applications*, 75(6):1868–1881, 2018.

[4] Slimane Adjerid, Nabil Chaabane, and Tao Lin. An immersed discontinuous finite element method for Stokes interface problems. *Computer Methods in Applied Mechanics and Engineering*, 293:170–190, 2015.

[5] Slimane Adjerid, Nabil Chaabane, Tao Lin, and Pengtao Yue. An immersed discontinuous finite element method for the Stokes problem with a moving interface. *Journal of Computational and Applied Mathematics*, 362:540–559, 2019.

[6] Slimane Adjerid, Ruchi Guo, and Tao Lin. High degree immersed finite element spaces by a least squares method. *International Journal of Numerical Analysis & Modeling*, 14(4-5):604–626, 2017.

[7] Ivo Babuška and Uday Banerjee. Stable generalized finite element method (SGFEM). *Computer methods in applied mechanics and engineering*, 201:91–111, 2012.

[8] Mohamed Ben-Romdhane, Slimane Adjerid, and Tao Lin. Higher-order immersed finite element spaces for second-order elliptic interface problems with quadratic interface. In *Advances in Applied Mathematics*, pages 171–178. Springer, 2014.

[9] Franco Brezzi and Michel Fortin. *Mixed and hybrid finite element methods*, volume 15 of *Springer Series in Computational Mathematics*. Springer-Verlag, New York, 1991.

[10] Erik Burman. Ghost penalty. *Comptes Rendus Mathematique*, 348(21-22):1217–1220, 2010.

[11] Waixiang Cao, Xu Zhang, and Zhimin Zhang. Superconvergence of immersed finite element methods for interface problems. *Advances in Computational Mathematics*, 43(4):795–821, 2017.

[12] Yuan Chen, Songming Hou, and Xu Zhang. An immersed finite element method for elliptic interface problems with multi-domain and triple junction points. *Advances in Applied Mathematics and Mechanics*, 11(5):1005–21, 2019.

[13] Yuan Chen, Songming Hou, and Xu Zhang. A bilinear partially penalized immersed finite element method for elliptic interface problems with multi-domain and triple-junction points. *Results in Applied Mathematics*, page 100100, 2020.

[14] Susanne Claus and Pierre Kerfriden. A CutFEM method for two-phase flow problems. *Computer Methods in Applied Mechanics and Engineering*, 348:185–206, 2019.

[15] Thomas-Peter Fries and Ted Belytschko. The Extended/Generalized finite element method: an overview of the method and its applications. *International journal for numerical methods in engineering*, 84(3):253–304, 2010.

[16] Sven Groß and Arnold Reusken. An Extended pressure finite element space for two-phase incompressible flows with surface tension. *Journal of Computational Physics*, 224(1):40–58, 2007.

[17] Ruchi Guo and Tao Lin. A higher degree immersed finite element method based on a Cauchy extension for elliptic interface problems. *SIAM Journal on Numerical Analysis*, 57(4):1545–1573, 2019.

[18] Ruchi Guo and Tao Lin. An immersed finite element method for elliptic interface problems in three dimensions. *Journal of Computational Physics*, 414(1):109478, 2020.

[19] Ruchi Guo, Tao Lin, and Yanping Lin. Error estimates for a partially penalized immersed finite element method for elasticity interface problems. *ESAIM: Mathematical Modelling and Numerical Analysis*, 54(1):1–24, 2020.

[20] Ruchi Guo, Tao Lin, Yanping Lin, and Qiao Zhuang. Error analysis of symmetric linear/bilinear partially penalized immersed finite element methods for Helmholtz interface problems. *arXiv preprint arXiv:2006.10942*, 2020.

[21] Ruchi Guo, Tao Lin, and Qiao Zhuang. Improved error estimation for the partially penalized immersed finite element methods for elliptic interface problems. *International Journal of Numerical Analysis & Modeling*, 16(4):575–589, 2019.

[22] Ruchi Guo and Xu Zhang. Solving three-dimensional interface problems with immersed finite elements: A-priori error analysis. *arXiv preprint arXiv:2004.08984*, 2020.

[23] Anita Hansbo and Peter Hansbo. An unfitted finite element method, based on Nitsche's method, for elliptic interface problems. *Computer Methods in Applied Mechanics and Engineering*, 191(47-48):5537–5552, 2002.

[24] Peter Hansbo, Mats G Larson, and Sara Zahedi. A cut finite element method for a Stokes interface problem. *Applied Numerical Mathematics*, 85:90–114, 2014.

[25] Cuiyu He and Xu Zhang. Residual-based a posteriori error estimation for immersed finite element methods. *Journal of Scientific Computing*, 81:2051–2079, 2019.

[26] Xiaoming He, Tao Lin, and Yanping Lin. Immersed finite element methods for elliptic interface problems with non-homogeneous jump conditions. *International Journal of numerical analysis and modeling*, 2011.

[27] Xiaoming He, Tao Lin, Yanping Lin, and Xu Zhang. Immersed finite element methods for parabolic equations with moving interface. *Numerical Methods for Partial Differential Equations*, 29(2):619–646, 2013.

[28] Alex Jarauta and Pavel Ryzhakov. Challenges in computational modeling of two-phase transport in polymer electrolyte fuel cells flow channels: A review. *Archives of Computational Methods in Engineering*, 25(4):1027–1057, 2018.

[29] Derrick Jones and Xu Zhang. A class of nonconforming immersed finite element methods for Stokes interface problems. *Journal of Computational and Applied Mathematics*, in revision, 2020.

[30] Derrick Jones and Xu Zhang. A conforming-nonconforming mixed immersed finite element method for unsteady stokes equations with moving interfaces. *submitted*, 2020.

[31] Raed Kafafy, Tao Lin, Yanping Lin, and Joseph Wang. Three-dimensional immersed finite element methods for electric field simulation in composite materials. *International journal for numerical methods in engineering*, 64(7):940–972, 2005.

[32] Matthias Kirchhart, Sven Gross, and Arnold Reusken. Analysis of an XFEM discretization for Stokes interface problems. *SIAM Journal on Scientific Computing*, 38(2):A1019–A1043, 2016.

[33] Philip Lederer, Carl-Martin Pfeiler, Christoph Wintersteiger, and Christoph Lehrenfeld. Higher order unfitted FEM for Stokes interface problems. *PAMM*, 16(1):7–10, 2016.

[34] Zhilin Li. The immersed interface method using a finite element formulation. *Applied Numerical Mathematics*, 27(3):253–267, 1998.

[35] Zhilin Li, Kazufumi Ito, and Ming-Chih Lai. An augmented approach for Stokes equations with a discontinuous viscosity and singular forces. *Computers & Fluids*, 36(3):622–635, 2007.

[36] Tao Lin, Yanping Lin, and Xu Zhang. Partially penalized immersed finite element methods for elliptic interface problems. *SIAM Journal on Numerical Analysis*, 53(2):1121–1144, 2015.

[37] Tao Lin, Yanping Lin, and Qiao Zhuang. Solving interface problems of the Helmholtz equation by immersed finite element methods. *Communications on Applied Mathematics and Computation*, 1(2):187–206, 2019.

[38] Tao Lin, Dongwoo Sheen, and Xu Zhang. A locking-free immersed finite element method for planar elasticity interface problems. *Journal of Computational Physics*, 247:228–247, 2013.

[39] Tao Lin, Qing Yang, and Xu Zhang. Partially penalized immersed finite element methods for parabolic interface problems. *Numerical Methods for Partial Differential Equations*, 31(6):1925–1947, 2015.

[40] Andrew Lundberg, Pengtao Sun, and Cheng Wang. Distributed Lagrange multiplier-fictitious domain finite element method for Stokes interface problems. *International Journal of Numerical Analysis & Modeling*, 2018.

[41] Benedikt Schott. *Stabilized cut finite element methods for complex interface coupled flow problems.* PhD thesis, Technische Universität München, 2017.

[42] Pengtao Sun. Fictitious domain finite element method for Stokes/elliptic interface problems with jump coefficients. *Journal of Computational and Applied Mathematics*, 356:81–97, 2019.

[43] C. Taylor and P. Hood. A numerical solution of the Navier-Stokes equations using the finite element technique. *An International Journal. Computers & Fluids*, 1(1):73–100, 1973.

[44] Cheng Wang, Pengtao Sun, and Zhilin Li. An iterative approach for constructing immersed finite element spaces and applications to interface problems. *International Journal of Numerical Analysis & Modeling*, 16(2), 2019.

[45] Nan Wang and Jinru Chen. A nonconforming Nitsche's extended finite element method for Stokes interface problems. *Journal of Scientific Computing*, 81(1):342–374, 2019.

[46] Qiuliang Wang and Jinru Chen. A new unfitted stabilized Nitsche's finite element method for Stokes interface problems. *Computers & Mathematics with Applications*, 70(5):820–834, 2015.

[47] Yuanming Xiao, Jinchao Xu, and Fei Wang. High-order extended finite element methods for solving interface problems. *Computer Methods in Applied Mechanics and Engineering*, 364:112964, 2020.

[48] Qing Yang. Numerical analysis of partially penalized immersed finite element methods for hyperbolic interface problems. *Numerical Mathematics: Theory, Methods & Applications*, 11(2), 2018.

[49] Qiao Zhuang and Ruchi Guo. High degree discontinuous Petrov–Galerkin immersed finite element methods using fictitious elements for elliptic interface problems. *Journal of Computational and Applied Mathematics*, 362:560–573, 2019.

Department of Statistics, The George Washington University, Washington, DC 20052, USA
E-mail: `yuan_chen@email.gwu.edu`

Department of Mathematics, Oklahoma State University, Stillwater, OK 74078, USA
E-mail: `xzhang@okstate.edu`